

A Data Driven Method for Model Based Diagnostics and Prognostics

Michael D. Bryant¹

¹, Mechanical Engineering, University of Texas at Austin, Austin, Texas 78712-0292
 bryantmd@austin.utexas.edu

ABSTRACT

This article’s model based diagnostics system has four modules. Diagnosis and fault location forms physics models of the machine, measures states off the real in-service machine, generates simulated machine states and simulated sensor outputs for the machine model with loads same as the real machine, and compares simulated sensor outputs to real sensor outputs. The parameter tuning module adjusts (tunes) the parameters of the model until the simulated sensor outputs closely mimic real sensor outputs. Tuning transfers information on the system’s health from the sensor data to the model’s parameters. Parameters changed from nominal values locate faults and bad parts. For the health assessment module to assess machine health, we view a machine as a “machine channel” that organizes power and information flow through the machine. Machines focus power via an organization inherent in its components and design. Broken or degraded components disrupt this organization and the power and information flows. Shannon’s information theory for communications channels can then be applied as a health metric to this “machine channel”. Ageing of components degrades machine functional health. To prognose future health, differential equations that model ageing of the machine’s components are formulated and solved. These equations predict component degradation, and update values of parameters in the model associated with component ageing. With these future parameter values, simulations of the machine operation model can then predict “future” machine behavior, and system health. This article demonstrates these methods on motors and a pump.

1. INTRODUCTION

A diagnostic system should detect, isolate, and identify the type and nature of a fault; determine the severity of the fault on system performance and the urgency of corrective action; analyze accommodation of the fault; and finally, forecast future behavior of the system, given the presence and future state of the fault. This article overviews a model based diagnostics and prognostics system, shown schematically in Fig. 1. The system integrates several modules developed at University of Texas at Austin into an overall diagnostics

Michael D. Bryant. This is an open-access article distributed under the terms of the Creative Commons Attribution 3.0 United States License, which permits unrestricted use, distribution, and reproduction in any medium, provided the original author and source are credited.

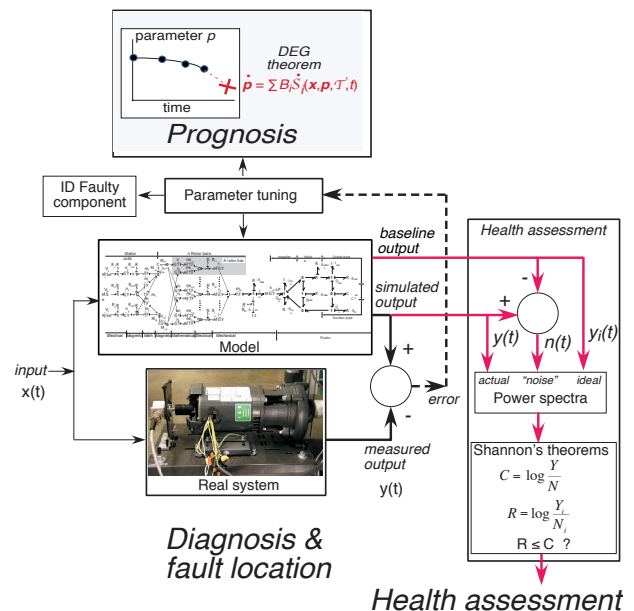


Figure 1. A schematic of the model based diagnostic system, consisting of four modules: diagnosis and fault location, consisting of real machine, inputs, sensor outputs, and physics model of machine; parameter tuning module to extract health condition from measurements; health assessment module to assess machine functional capability; and prognosis module to forecast future machine condition.

system. The modules described in the next section were all developed from fundamentals of physics and information theory.

Model-based diagnostics constructs models of machines to interpret sensor signals in terms of faults and locate and track faults in machines. Figure 1 depicts the system consisting of real machine; inputs to the machine; a physics based model of the machine with many physical states and parameters; outputs from the machine measured by sensors, and corresponding outputs simulated by the model; a module that tunes or adjusts the numerical values of the

model's parameters to make the model's simulated outputs mimic the real machine's measured outputs; a health assessment module to evaluate the system's health or ability to do a job using the measured signals; and a prognosis module which forecasts the changed values of parameters of an aged machine, via a thermodynamics based method of modeling effects of degradation. With these future "aged" parameters, the model can simulate future machine behavior to predict the future health condition of the machine. In the following sections, the components and operation of each module will be described in detail.

Since these modules are all based on fundamentals of physics and information theory, the reliability of this overall diagnostics system is extremely high.

2. MODEL BASED DIAGNOSTIC SYSTEM

Each module of Fig. 1 will be introduced and described.

2.1. Diagnostics and Fault Location Module (DFLM)

In Fig. 1, the Diagnostics & fault location module consists of a sensory system to observe the real machine and faults, and a detailed physics based model of the machine system to interpret the sensor signals. The model simulates the behavior of both machine and sensor system.

2.1.1. Sensor System and Observability

For any diagnostics system to work properly, the sensors must collect sufficient, correct and appropriate information from the system. The sensor system must be observable to the faults.

Model based diagnostics do not require exotic sensors. Simple and common sensors found on industry machines can usually ensure diagnosability. Although models interpret the sensor signals, these signals must contain sufficient information to enable a correct diagnosis. For motors, typically measured are voltages, currents, run-outs, speed, vibration and temperature by sensors such as potential/current transformer, hall-effect sensor, capacitive probe, encoder, accelerometer, and thermocouple. Key to selecting the right combination of sensors with enough information to detect a fault is fault observability, which in this context measures how well parameters can be inferred from information contained in error signals of model outputs and measurements (Analytic Sciences Corporation, 1974).

A dynamic system model is required to assess observability of a sensor system to any state or signal in a machine, such as a fault-induced signal. Nakhaeinejad & Bryant (2011) assessed observability to faults for an AC motor. Alternatively, sensitivity of sensor signals to changes in a fault can be studied, as Bryant, Nakhaeinejad & Choi (2011) did for the motor pump system presented in this article.

2.1.2. System Model

The model interprets the complex sensor signals. The model consists of differential equations that govern the physics of the machine. The model based diagnostic system of this article employs extremely detailed physics based models with direct physical correspondence between elements in the model and components and faults in the real machine. All relevant physics and effects are embedded in the model. Although this imbues the model with many degrees of freedom, many states, a high dynamic order, very many system parameters, and extreme nonlinearities, *this complexity is required in the model to interpret the equally complex sensor data*, which contains multiple competing signals from the many components and physical effects in a real machine. For example, in a motor, the bearing vibration signals measured by accelerometers are contaminated with vibrations from the motor's rotor reacting to harmonics of the magnetic field. These vibrations have harmonic components similar to the bearing, which confounds signal based bearing diagnostics.

During a simulation of the machine model, the model is given the same inputs as the real machine, see Fig. 1. Simulations attempt to emulate the real machine's dynamic states, up to and including the sensor measurements. Note the model contains a model of the sensor behavior. Signals measured off the real machine by sensors are then compared to corresponding signals derived from simulations of the model. For simulations to emulate real machine behavior, i.e., for the model's outputs to match the real machine's outputs, the model's parameters are tuned—adjusted until simulated outputs overlay measured outputs. This is the function of the parameter tuning module.

2.2. Parameter Tuning Module (PTM)

The parameter-tuning module accepts sensor signals from the real machine, and commands a simulation of the model. Initially, the model's parameter values are those of a healthy machine¹. The simulation, given the same inputs as the real machine, computes system states up to and including the (simulated) sensor measurements. The parameter-tuning module subtracts the simulated sensor outputs from the corresponding measured sensor outputs, Fig. 1, and constructs an error function as the sum of the differences squared. Minimization of this error function drives an iterative process that corrects those parameters of the model associated with the known faults that compromise operation. Industry usually knows where and how faults occur in their machines, unknown is when the fault will occur. Parameter tuning performs simulations with updated parameters until the error function is within an acceptable tolerance. To

¹ These healthy machine parameters can be estimated via a combination of the machine's design specs and/or tuning of parameters using a baseline signal that exemplifies health.

reduce computational load, only tuned are those parameters associated with the machine's faults and ageing, which cause the measured signals to change.

If the model's parameters have a direct physical correspondence to components and faults in the real machine, tuning of parameters until simulations emulate real machine behavior extracts and puts the health condition information from the sensor signals into the parameter values of the model. Since the model's parameters have a direct physical correspondence to components and faults in the real machine, the tuned parameter values locate the fault and inform on its severity, via how much the parameter(s) have changed from nominal healthy values. If the model is physics based, the updated parameter values are easily interpreted in terms of physical effects of faults. This removes the pattern classification and training problem usually associated with heuristic and signal based diagnostic systems.

The parameter tuning module is challenged by the quality of the sensor data, which is compromised by noise and inadequate observability. Measurements inherently include sensor and physical process noise, and observability of a measurement can vary markedly if the system is nonlinear. To address these challenges, we tried online tuning with Kalman and Extended Kalman filters, and offline tuning with an algorithm that minimizes global errors. A Kalman filter augments a physics model with a statistical model of the noise, for more accurate estimates of states (Haykin, 2001). Kalman filters first predict future states, and then correct these states recursively, using the error between simulation and measurement, and a Kalman gain, which arises from the analytical solution to the error minimization problem. For nonlinear systems, the extended Kalman filter includes the parameters to be tuned as extra components in the state vector. This usually results in a more nonlinear system, because the governing differential equations—the system differential equations augmented with equations that describe parameter degradation—usually involve products of parameters and states.

The Kalman filters operating with the detailed physics models described earlier operated satisfactorily in the presence of noise, but often failed due to observability issues associated with the nonlinear nature of the models. Sensors observability of faults can reduce and even vanish due to the nonlinearities of machine models (Nakhaeinejad & Bryant, 2011). A Kalman filter sequentially processes a signal point by point and must “latch on” to the signal. When extreme nonlinearities reduced sensor observability, the Kalman filter would detach from the signal, and become unstable. An offline tuning method was much less affected by this waning observability issue.

The offline tuning method (Rengarajan, 2010) constructs a multi-dimensional parameter space, with each parameter to

be tuned assigned a coordinate axis. Thus N parameters require an N dimensional space, and tuning the set of parameters is tantamount to searching for the correct point in the space. The search is limited to those regions of the space where parameter values are physically possible or reasonable. First, a deterministic sampler scans the entire admissible region, without bias to any particular sub-region, using a grid. At each sampling point, error residuals between measured sensor signals and model simulated sensor signals are calculated to identify five regions where residuals are smallest. Then a “Non-Dominating Sorting Genetic Algorithm” is run in small regions about the five zones to pinpoint the global minimum. This algorithm involves randomness, to maximize the likelihood of attaining a global minimum in case the deterministic sampler gets stuck in local minima. The resulting global minimum values are ranked, and the top candidate is used as the system parameter values. Tuning is iterative and ends once error tolerances are met.

The offline tuner was tested on a DC motor where the created rotor bar resistance faults were known (Rengarajan, 2010). Tuned parameters included rotor inertia, motor constant, rotor bar resistance, and damping coefficient. Motor speed was varied by suitably adjusting the input voltage. The tuning algorithm estimated the rotor bar resistance values using motor speed measurements to within a few percent.

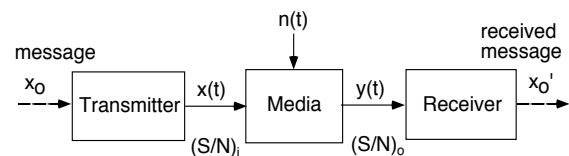


Figure 2. Shannon & Weaver (1948) communications channel.

2.3. Health Assessment Module (HAM)

The health assessment module determines the functional health capability of the machine, based on the channel capacity C from Shannon's information theory. Shannon's C is the maximum amount of information x_0 in bits per second that can be transmitted through a channel contaminated with noise, but yet received without error. Shannon's theory, which specifies signal to noise power ratios Y/N and channel bandwidth ω , has underpinned all communication systems design since 1948. Obey Shannon's theorems and a system works, otherwise not.

The Shannon & Weaver (1948) channel capacity for a time continuous channel with white Gaussian noise in Fig. 2 is

$$C = \omega \log_2 \left(\frac{Y}{N} \right) \quad (1)$$

which involves average power

$$Y = P\{y(t)\} = \frac{1}{T} \int_0^T [y(t)]^2 dt \quad (2a)$$

of signal $y(t) = x(t) + n(t)$, and power of noise $n(t)$,

$$N = P\{n(t)\} = \frac{1}{T} \int_0^T [n(t)]^2 dt \quad (2b)$$

In Fig. 2, the received signal $y(t)$ is the transmitted signal $x(t)$ corrupted with noise $n(t)$ from the channel. Here bandwidth ω (Hz) of the channel is usually determined via Nyquist's rules.

A machine will be viewed as a "machine communications channel" with input signals transmitted over a "machine channel" and received as the machine's output signals. Here faults create and add "fault noise" to output signals. To apply Shannon's fundamental theorems to assess machine health, noise will be defined as

$$n_i(t) = y(t) - y_i(t), \quad (3)$$

the difference between output $y(t)$ of the degraded machine, and a baseline signal $y_i(t)$ that exemplifies health, as discussed in Costuros & Bryant (2014). The noise signal of Eq. (3), a residual between degraded $y(t)$ and baseline $y_i(t)$, contains the "fault noise" signals generated by faults, and random sensor and system noise present in both $y(t)$ and $y_i(t)$. Of course, to use Eq. (3) in an industry setting, signals $y(t)$ and $y_i(t)$ must first be correlated in time to have the same starting point and be synchronized.

Applying Eqs. (2) to baseline signal $y_i(t)$ and noise $n_i(t)$ of Eq. (3) produces a channel capacity for the baseline signal

$$R = \omega_i \log_2 \left(\frac{Y_i}{N_i} \right) \quad (4)$$

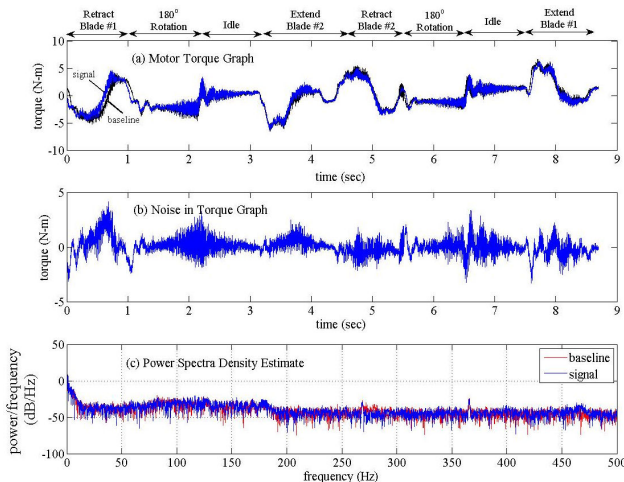


Figure 3. Motor torque response from robot 1 on 1/15/10.

Here bandwidth ω_i of baseline signal $y_i(t)$ is usually equal to ω . Equation (4) will be used in place of Shannon's rate of information in Shannon's test channel health, wherein if

$$R \leq C, \quad (5)$$

the system will satisfactorily perform its function, otherwise not. Costuros (2013) showed that unless the power of sensor and system noise overwhelms ($> 20\%$) the fault noise, the test of Eqs. (1)–(5) will work in an industry setting.

Costuros & Bryant (2014) demonstrated the efficacy of channel capacity as a health metric via tests on ageing industry robots, which will be reviewed here. The channel capacity technique was tested on eight DC motors in four industry robots, each initially in good operating condition. An identical sequence of voltage steps (transmitted channel inputs) were repetitively applied to all motors, and torque signals $y(t)$ (received channel outputs) were then collected from all motors. Motors ran continuously from 12/9/09 to 2/5/10. Motor output torques were measured on 12/9, 12/18, 1/15, 1/21 and 2/5. The 12/9 measurements were designated as baseline signals $y_i(t)$ exemplary of good health, to which all subsequent measurements $y(t)$ on the same motor were compared. Before any calculations, a signal $y(t)$ was first correlated to its $y_i(t)$ to synchronize signal alignments in time. Figure 3a shows robot 1 motor torque $y(t)$ on 1/15 (blue curve), and its baseline $y_i(t)$ (black curve). Fault noise in Fig. 3b obtained via Eq. (3) distills the fault induced signal from $y(t)$. Power spectra of signal $y(t)$ and noise $n_i(t)$ computed via Eq. (3) are in Fig. 3c. Channel capacity C was estimated via Eq. (1) and tabulated in Table 1.

Table 1: Channel capacity for motors of robots vs. time.

Date	Robot 1		Robot 2		Robot 3		Robot 4	
	Motor A	Motor B	Motor A	Motor B	Motor A	Motor B	Motor A	Motor B
12/18/09	2193	2164	1780	2326	1878	1647	2051	1679
1/15/10	1965	1784	1335	1481	1307	964	1383	989
1/21/10	2039	1827	1375	1466	1465	1072	1406	1005
2/5/10	1907	1985	1188	1340	1252	929	1475	1043
% change 12/18 - 1/15	10% BEST	18%	25%	36% WORST	30%	41%	33%	41%
	1	2	3	8	4	6	5	7
% change 12/18 - 1/21	7% BEST	16%	23%	37% WORST	22%	35%	31%	40%
	1	2	3	8	4	5	6	7
% change 12/18 - 2/5	13% BEST	8%	33%	42% WORST	33%	44%	28%	38%
	2	1	4	8	5	7	3	6

For measurements after 12/18, fractional changes in channel capacity $\%C = 1 - C/C_{12/18}$ relative to values for 12/18 measurements were tabulated in Table 1 for all motors. Inspection of the upper rows reveals a trend of diminishing channel capacity over time. For example, for motor B of robot 2, C diminishes from 2,326 to 1,340 from 12/18/09 to

2/5/10. In subsequent rows, the percent change of channel capacity from 12/18 to 1/21 is displayed, along with a composite of human produced evaluations of motion performance by a team of industry engineers and technicians. The human evaluations rank-ordered the motors and identified the best and worst performing motors. In general, the channel capacity estimates agreed well with human (team) assessments. Motor ‘A’ in robot 1, deemed BEST by the team, had the smallest channel capacity reductions. Motor ‘B’ in robot 2, rated WORST by the team, consistently showed the largest reduction of channel capacity and was prematurely removed from service due to development of a grinding noise. In general, the drop in the channel capacity values correlated very well with the human perceived amount of motor degradation. An overall decline in channel capacity indicates degradation. This application suggests that the channel capacity metric can quantify system degradation in industry settings. The channel capacity decreases in Table 1 are not strictly monotonic. Fluctuations in the C values in Table 1 for most motors at the beginning of tests are consistent with a break-in process, wherein performance does vary. For these motors, the majority of faults occurred on the motor bearings due to lubrication breakdown.

2.4. Prognosis Module (PM)

The prognosis module, schematically shown at the top of Fig. 1, forecasts future values of the model’s parameters via differential equations that govern the ageing and degradation of the system’s components. These equations and the ageing phenomena typically have time constants much larger than the characteristic times of the machine in operation. To make the Prognosis module compatible with the other diagnostic modules, the component degradation equations are posed in terms of those system parameters P_k that change due to component degradation. This degradation or ageing worsens the faults. Equations that govern degradation (Bryant, 2014) can be formulated via the Degradation Entropy Generation theorem (Bryant, Khonsari & Ling, 2008), which equates the rate of change of a variable w that measures the degradation (i.e., monotonically increases or decreases as the fault becomes more severe) to a linear combination of the irreversible entropies S_i' generated by the n dissipative processes underlying the degradation, i.e.,

$$\frac{dw}{dt} = \sum_{i=1}^n B_i \frac{dS_i'}{dt} \quad (6a)$$

Equation (6a) is founded on the laws of thermodynamics. Although the B_i constants are usually unknown, the irreversible entropies S_i' on the right side of Eq. (6a) can be formulated in terms of the power dissipated by components, divided by a temperature associated with the degradation, using knowledge of the mechanics of dissipation losses and the ageing and degradation mechanisms. If degradation

changes parameter P_k then $P_k = P_k(w)$, and via the chain rule $dP_k/dt = dP_k/dw (dw/dt)$. Substitution of Eq. (6a) gives

$$\frac{dP_k}{dt} = \sum_{i=1}^n \left(B_i \frac{dP_k}{dw} \right) \frac{dS_i'}{dt} = \sum_{i=1}^n B_i^* \frac{dS_i'}{dt} \quad (6b)$$

where dP_k/dw was grouped with the constants B_i to form new constants B_i^* . Values for these constants can be obtained via the tuning module, since a history of values for parameters P_k will be available from past tunings of the operational model to sensor data.

Over the course of multiple tunings, a record of the parameter’s values P_k versus time can be constructed, as in the graph seen in the Prognosis section of Fig. 1. Future values of parameters P_k , associated with faults could be forecast by fitting a curve through the record of P_k data points, and extrapolating that curve into the future, as in point “X”. A more accurate forecast uses Eqs. (6b) and tunes the unknown constants B_i^* with the record of P_k versus time. Then using the most recent value of P_k as an initial condition, the P_k can be forecast much further into the future. With future values for the parameters P_k , the machine model shown in Fig. 1, given the machine’s inputs, can now simulate the future degraded machine behavior and its output signals $y(t)$. With these future output signals $y(t)$ inserted into Eq. (3), the health assessment module can assess future machine performance.

2.5. Diagnostic System Operation

The diagnostic system operates as follows. Abbreviations are defined in the headings of section 2.

- 1) DFLM simulates the model of Fig. 1 with inputs same as the service loads on the real machine, and outputs including the sensor states.
- 2) DFLM compares simulated “sensor” signals to the real sensor measured signals.
- 3) PTM adjusts (tunes) the model’s parameters, until simulated sensor readings overlay real sensor readings. Accuracy is a few percent. The tuned model now emulates machine behavior, and distilled into the tuned parameter values is the machine’s health condition.
- 4) PTM detects and locates faults by tracking changes in the numerical values of the tuned parameters. Larger changes implies a more severe fault(s).
- 5) HAM compares the machine’s signals $y(t)$ to a baseline signal $y_i(t)$ that exemplifies machine health, and assesses machine condition by calculating the machine channel capacity C , and the percent change from baseline channel capacity.
- 6) PM with the history of the model’s parameters from past tunings, solves the differential equations governing parameter change, and predicts future parameter values.

- 7) **DFLM** simulates the model of the “future” machine with inputs same as past service loads on the real machine, and outputs “simulated sensor” states to predict future machine operation.
- 8) **HAM** compares the “future” machine signals $y(t)$ to the baseline signal $y_i(t)$, and calculates the channel capacity of the future machine to assess future machine condition.

3. MOTOR PUMP APPLICATION

The techniques discussed in section 2 will be demonstrated on a centrifugal pump driven by an induction motor, Fig. 4. Faults introduced include extra resistance in the motor’s stator circuit and blockage in the pipe following the pump.

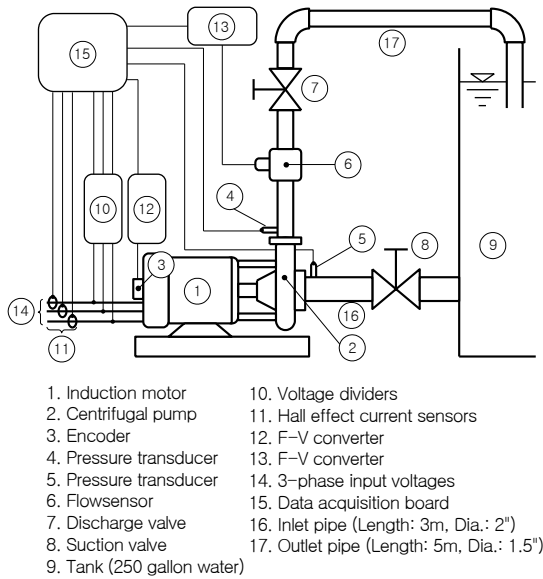


Figure 4. Motor-pump system test setup.

3.1. Motor Pump Model

Within the **DFLM** module in Fig. 1, in the block labeled “model” is a bond graph model of the dynamics of a squirrel cage induction motor driving a centrifugal pump. From the bond graph, differential equations governing motor-pump operation were extracted and presented in Bryant & Choi (2012). The model has parameters with nominal values listed in Table 2.

In Fig. 4, a 3-phase, 2 hp, 3600 rpm squirrel cage induction motor (1) drives a centrifugal pump (2) (19 m max. head). Measured are 3 phases of input voltage (10), 3 phases of currents (11) via Hall effect sensors, motor rotational speed (3), flow rate at the outlet pipe (6), and pressures at inlet (5) and outlet (4) of the pump via pressure transducers.

Table 2 Parameters of motor-pump, with nominal (healthy system) values.

Parameters	Description	Healthy value
R_s	Stator coil resistances (Ω)	1.0281
R_{sm}	Stator magnetic losses ($1/\Omega$)	366.7
$R_{r1} \dots R_{r34}$	Rotor bar resistance (Ω)	0.8663
L_s	Stator inductances (H)	0.1033
L_r	Rotor inductances (H)	0.1377
L_m	Mutual inductances (H)	0.1162
R_{br}	Mechanical friction (N-s/m)	0.0034
R_{disk}	Mechanical friction (N-s/m)	1.1e-5
R_{imp}	Loss in impeller (kg/m^2)	3.6e11
R_{volute}	Loss in volute (kg/m^2)	7.0e9
R_{leak}	Leakage loss (kg/m^2)	1.6e15
R_{out}	Loss in outlet pipe (kg/m^2)	2.3e11
R_{in}	Loss in inlet pipe (kg/m^2)	1.0e10
J	Moment of inertia (N-m^2)	0.003802
I_{imp}	Liquid inertia in impeller (kg/m^5)	8.6e7
I_{out}	Liquid inertia in outlet pipe (kg/m^2)	2.5e6
n_s	Number stator coil turns	111
n_r	Number rotor coil turns	1
r_{i1}	Impeller inner radius (m)	0.025
r_{i2}	Impeller outer radius (m)	0.05
B_{i1}	Axial width at impeller inlet (m)	0.01
B_{i2}	Axial width at impeller outlet (m)	0.01
β_1	Blade angle at impeller inlet ($^\circ$)	15
β_2	Blade angle at impeller outlet ($^\circ$)	30

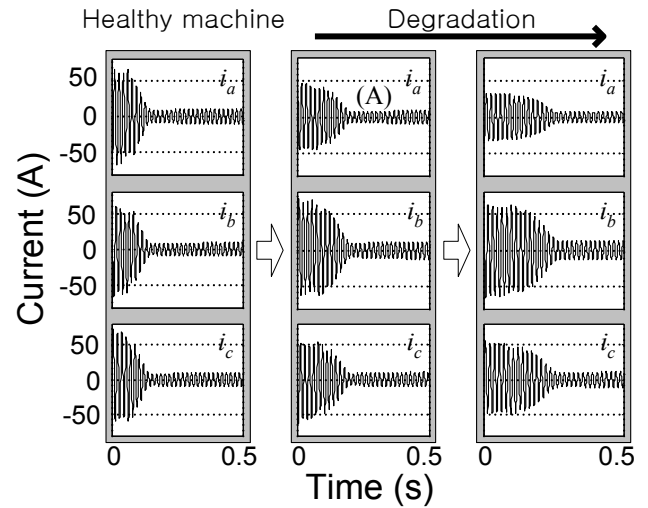


Figure 5. Currents in (a) healthy motor, and with extra resistance (b) 2.5Ω and (c) 4.5Ω in phase a of stator.

For the stator circuit fault, Fig. 5 shows the change of measured 3 phase currents (a , b , c), from healthy to degraded. The (b) and (c) subfigures in Fig. 5 connected 2.5Ω and 4.5Ω in series to the a phase stator coil. As the resistance fault increases, the time to steady state increases, and magnitudes of i_a reduce. Higher resistance

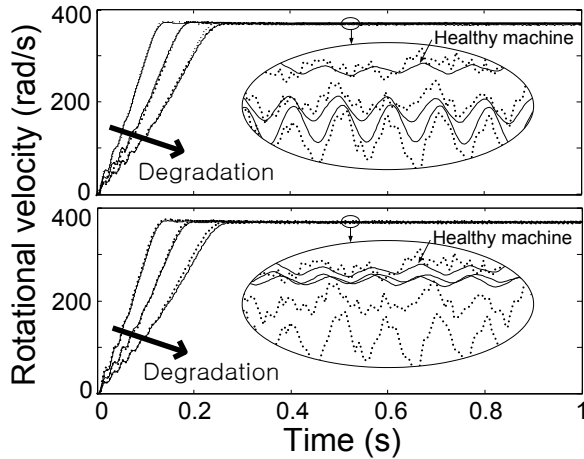


Figure 6 Measured (dotted lines) and tuned (solid lines) rotational velocity by stator coil resistances (upper) and by motor inductances (bottom).

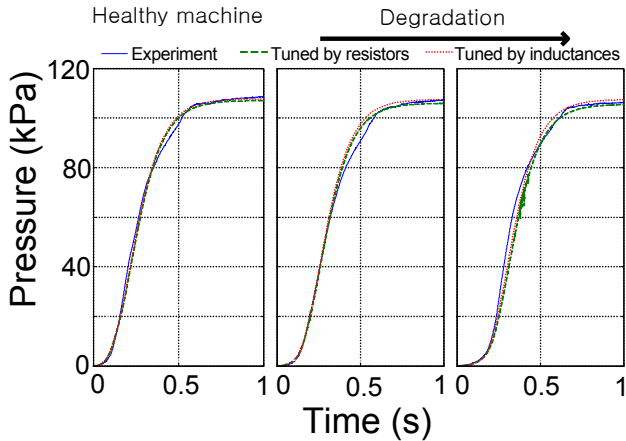


Figure 7 Pressures for a) healthy, (b) 2.5 Ω , (c) 4.5 Ω .

simultaneously affected measured current, rotational velocity, and pressure, Figs. 6 and 7.

Table 3 assesses sensitivity of measured states to changes in selected parameters, as substitute for an observability assessment of the sensor system. After each parameter in table 2 was individually perturbed 1% of nominal value, a simulation was performed to observe changes in system response. The number of '+' symbols in any row in table 3 indicates the influence of each parameter's change. Measured currents, rotational velocities, and pressures are sensitive to changes in stator coil resistances (R_{sa} , R_{sb} , R_{sc}) or motor inductances (L_s , L_r , L_m), even though the origin of the fault is the stator resistance R_{sa} . First, the motor-pump model was tuned by adjusting stator coil resistances only, and tuned a second time by adjusting motor inductances only. The error function for tuning was the sum of the square of differences between measured and simulated

rotational velocity. Currents and pressures were not considered in the error function. Simulations of healthy (Table 2) and degraded machines (Table 4 presented in Figs. 6, 7, and 8) nearly overlay experiments. Although Figures 7 and 8 tuned parameters so that rotational velocity simulations overlaid measurements, as a by-product, current and pressure simulations also overlaid their respective measurements.

Table 3 Sensitivity of system states to 1% change in parameters.

Parameters	Sensitivities		
	Rotational speed	Currents	Pressure (Flow rate)
R_s	++	+++	++
R_{r1}, \dots, R_{r34}	.	+	.
L_s, L_r, L_m	+++	+++	+++
R_{bp}, R_{disk}	++	+	+
R_{imp}	.	.	++
R_{out}	.	.	++
$R_{in}, R_{volute}, R_{leak}$.	.	.

Simulations with parameters tuned by stator coil resistances and by motor inductances gave similar rotational velocities (Fig. 6) and pressures (Fig. 7). However, the magnified details shown in the bubbles in Fig. 6 of rotational velocities at steady state suggests that simulations from tuning by stator coil resistances more closely fits measurements, than tuning by motor inductances, for the resistance fault. Since the induction motor model represents a symmetrical electric machine, each of R_{sa} , R_{sb} , and R_{sc} with the tuned values can in turn produce the rotational velocities in Fig. 6. The magnitude of currents i_a in Fig. 5 reduce most as the value of connected resistor R_{sa} increases. Other currents (i_b and i_c in Fig. 5) change only little. Thus R_{sa} has to be the largest among the tuned resistances. Fig. 8 compares simulated to measured current i_a (Fig. 5), after assigning the largest value

Table 4 Parameter tuning data.

Parameters		Healthy value	Connected resistor	
			2.5 (Ω)	4.5 (Ω)
Tuning by resistances	R_{sa} (Ω)	1.0281	2.0525	5.0668
	R_{sb} (Ω)		1.0959	1.3719
	R_{sc} (Ω)		0.5296	1.3931
Tuning by inductances	$L_{s\alpha}$ (H)	0.1033	0.1037	0.1041
	$L_{s\beta}$ (H)		0.1031	0.1037
	$L_{r\alpha}$ (H)	0.1377	0.1382	0.1387
	$L_{r\beta}$ (H)		0.1379	0.1382
	$L_{m\alpha}$ (H)	0.1162	0.1152	0.1143
	$L_{m\beta}$ (H)		0.1154	0.1148

Subscripts a , b , c , α , and β denote magnetic axes.

of tuned stator coil resistance to R_{sa} .

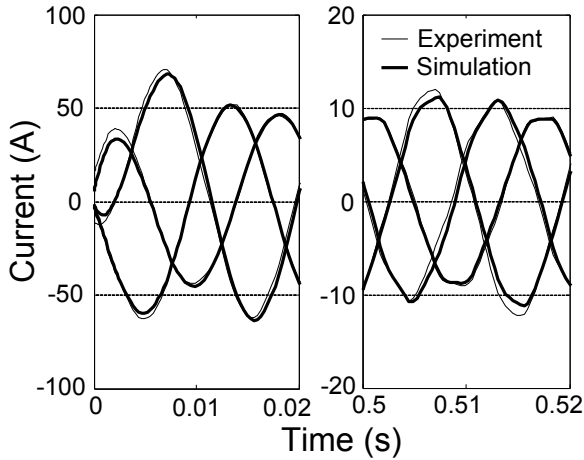


Figure 8. Magnified view of current (A) in Fig. 5 with tuned response after adjusting stator coil resistances.

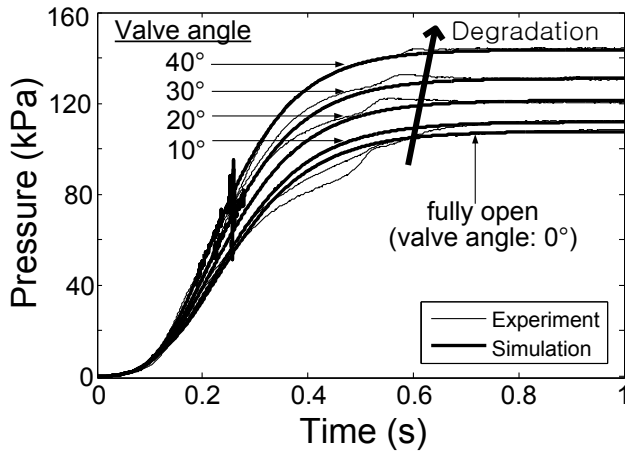


Figure 9. Tuned pressures by hydraulic loss at outlet pipe, R_{out} .

Fluid loss, R_{out} in the centrifugal pump model models pipe line losses such as friction loss, expansion loss, contraction loss, valve loss, etc. The butterfly valve (7) of Fig. 4 in the middle of the outlet pipe was closed in 10° increments to mimic increasing resistance. The valve can be adjusted from fully open 0° to fully closed 90° . Closing the valve from 0° to 40° had little effect on measured currents and rotational velocity, but pressure signals increased significantly. From Table 3, R_{out} was selected as the parameter for tuning, since it increases outlet pressure significantly, with little effect on currents and rotational velocity. R_{imp} was deselected, since increasing R_{imp} decreases outlet pressure. Figure 9 shows the measured pressure as valve angle changed from 0° to 40° , and the simulated pressure obtained by adjusting R_{out} from

2.3×10^{11} , to 2.4×10^{11} , 2.7×10^{11} , 3.1×10^{11} , and 3.3×10^{11} (kg/m^7). Changing R_{out} had negligible effect on current and rotational velocity, as implied by Table 3.

The channel capacity C for measured outputs of stator phase current i_a and motor speed ω were calculated via Eq. (1) and presented versus resistance in stator phase a in Fig. 10. Values were normalized by maximum values, so the largest C value is one. As the fault worsens and system performance degrades as shown in Figs. 5 and 6, the channel capacity monotonically diminishes, similar to that of Table 1.

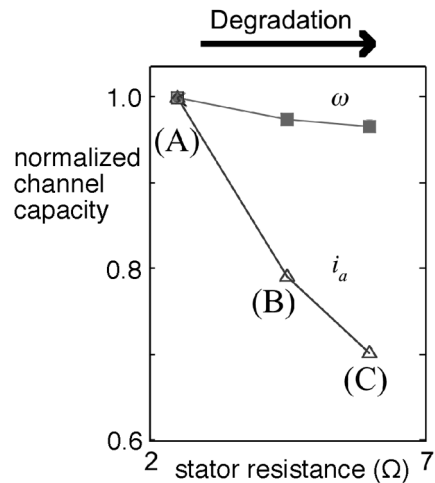


Figure 10. Channel capacity vs. stator a resistance.

4. CONCLUSION

A model-based diagnostic system was presented, with application to a motor-pump. Physics models of high detail and fidelity permitted simulations to match experiments with marginal error. Parameter tuning selected values of parameters such that simulations overlaid measurements. Contained in the tuned values of parameters is the machine health condition. The channel capacity health metric assessed fault severity. For signals over channels through a machine that possess observability of the fault(s) in question, this article shows that models and parameter tuning can locate and isolate faults. For signals observable to a given fault, channel capacity monotonically diminished with severity of the fault.

ACKNOWLEDGEMENT

Research reported in this publication was supported in part by the National Science Foundation (NSF) grant IIP 1266279. The content is solely the responsibility of the

authors and does not necessarily represent the official views of the National Science Foundation.

REFERENCES

- Analytic Sciences Corporation. Technical Staff & Gelb, A., (1974). *Applied Optimal Estimation*. Cambridge, MA: M.I.T. Press.
- Bryant, M.D., (2014). Modeling Degradation Using Thermodynamic Entropy, submitted to PHM 2014 Conference.
- Bryant, M.D., Khonsari, M.M. & Ling, F.F. (2008). On the thermodynamics of degradation, *Proceedings of Royal Society of London Series A*, vol. 464 (2006), pp. 2001-2014, doi:10.1098/rspa.2007.0371.
- Bryant, M.D., & Choi, J.H. (2012). Model based fault diagnostics of induction motor and centrifugal pump, *Proceedings of MFPT 2012 Conference*. April 24- 26, Dayton, OH.
- Bryant M.D., Nakhaeinejad M. & Choi J., (2011). Model based diagnostics and fault assessment of induction motors with incipient faults, *Proceedings of the Society for Experimental Mechanics Series*, vol. 8, pp. 439 – 449.
- Costuros T., (2013). *Application of Communication Theory to Health Assessment, Degradation Quantification, and Robot Cause Diagnosis*, Doctoral dissertation, University of Texas at Austin, Austin, TX, <https://repositories.lib.utexas.edu/bitstream/handle/2152/21566/COSTUROS-DISSERTATION-2013.pdf>.
- Costuros, T. & Bryant, M.D. (2014). Application of information theory's channel capacity as an industry machine health and diagnostic metric. *Proceedings of MFPT 2014 Conference*. May 19-22, Virginia Beach, VA.
- Haykin, S. S. (2001). *Kalman Filtering and Neural Networks*. New York: Wiley.
- Nakhaeinejad, M. & Bryant, M. D., (2011). Observability Analysis for Model-Based Fault Detection and Sensor Selection in Induction Motors, *Journal of Measurement Science and Technology*, vol. 22(7), pp. 075202.
- Rengarajan, S.B., (2010). A Method for Parameter Estimation and System Identification for Model Based Diagnostics Masters Thesis, University of Texas at Austin, Austin, TX.
- Shannon, C.E. & Weaver, W., (1948). *The Mathematical Theory of Communication*, Urbana, IL: The University of Illinois Press.
- Shannon C. E. (1949). Communication in the presence of noise, *Proceedings of the IRE*, vol. 37, pp. 10 – 21.

BIOGRAPHY

Michael D. Bryant, Accenture Endowed Professor of Mechanical Engineering at University of Texas at Austin, Austin TX, USA, was born in Danville IL on Feb. 8, 1951. His education includes B.S., Bioengineering, University of Illinois at Chicago, Chicago, IL, USA, 1972; graduate study in Information Engineering, University of Illinois at Chicago, 1972-1974; M.S., Mechanical Engineering, Northwestern University, Evanston, IL, USA, 1980; and Ph.D., Engineering Science and Applied Mathematics, Northwestern University, 1981. He has been with University of Texas at Austin since 1988. From 1981-1988 he was an Assistant and Associate Professor at North Carolina State University. His interests include tribology, mechatronics, manufacturing, and system modeling. He is a fellow of American Society of Mechanical Engineers, was Editor in Chief of ASME Journal of Tribology from 2005-2012, and is a member of Institute of Electrical and Electronics Engineers and Sigma Xi.

